



# PartRAG: Retrieval-Augmented Part-Level 3D Generation and Editing

Peize Li<sup>1\*</sup> Zeyu Zhang<sup>2\*†</sup> Hao Tang<sup>2‡</sup>

<sup>1</sup>King’s College London <sup>2</sup>Peking University

\*Equal contribution. †Project lead. ‡Corresponding authors: bjdxtanghao@gmail.com.



Figure 1. **PartRAG at a glance.** Each row shows three stages: *left column*—textured input image; *middle column*—generated part-structured 3D meshes with crisp boundaries (shown as gray models); *right column*—decomposed individual parts, enabling localized, view-consistent editing. Our retrieval-augmented framework reconstructs part-structured 3D assets across diverse categories and maintains parts in a shared canonical space for interactive manipulation.

## Abstract

*Single-image 3D generation with part-level structure remains challenging: learned priors struggle to cover the long tail of part geometries and maintain multi-view consistency, and existing systems provide limited support for precise, localized edits. We present PartRAG, a retrieval-augmented framework that integrates an external part database with a diffusion transformer to couple generation with an editable representation. To overcome the first challenge, we introduce a Hierarchical Contrastive Retrieval module that aligns dense image patches with 3D part latents at both part and object granularity, retrieving from a curated bank of 1,236 part-annotated assets to inject diverse, physically plausible exemplars into denoising. To overcome the second challenge, we add a masked, part-level editor that operates in a shared canonical space, enabling swaps, attribute refinements, and compositional updates without regenerating the whole object while preserving non-target parts and multi-view consistency. PartRAG achieves competitive results on Objaverse, ShapeNet, and ABO, reducing Chamfer Distance from 0.1726 to **0.1528** and raising the F-Score from 0.7472 to **0.844** on Objaverse, with an inference time of 38s and interactive edits in 5–8s. Qualitatively, PartRAG produces sharper part*

*boundaries, better thin-structure fidelity, and robust behavior on articulated objects. Code: <https://github.com/AIGeeksGroup/PartRAG>. Website: <https://aigeeksgroup.github.io/PartRAG>.*

## 1. Introduction

Part-aware 3D assets underpin applications ranging from immersive content creation to robotic manipulation, yet generating editable meshes from a single image remains demanding. Recent diffusion-style transformers such as PartCrafter [20] and OmniPart [37] improve compositional generation by denoising all parts jointly, while segmentation-then-reconstruct pipelines [4, 22, 36] leverage 2D priors to bootstrap part masks. Despite these advances, purely generative priors still struggle to cover the long tail of part geometries, and their outputs lack the explicit control needed for downstream editing.

We identify two fundamental challenges when applying current systems in production pipelines. *First*, limited diversity in the learned priors leads to implausible geometry and view-inconsistent details whenever the query object deviates from frequent training patterns; for example, our reproduction of PartCrafter exhibits 32% of its residual errors on complex articulations (Chamfer Distance (CD) =

0.2134) and 28% on thin structures ( $CD = 0.1876$ ), revealing brittle coverage of rare layouts. *Second*, existing generators provide little support for precise, part-level editing: users cannot selectively replace or adjust subcomponents without destabilizing the whole asset, making localized design iterations laborious.

To overcome the first challenge, we introduce *PartRAG*, a retrieval-augmented framework that couples generation with an editable representation. We design a Hierarchical Contrastive Retrieval (HCR) module that aligns 2D image patches with 3D part latents at both object and part granularity, indexing a curated database of **1,236** reference assets to inject diverse, physically plausible exemplars. The retrieval module employs a bidirectional momentum queue mechanism (Algorithm 1) to maintain a large pool of negative samples during contrastive learning, and integrates retrieved part tokens into a dual-lane diffusion transformer backbone via retrieval cross-attention. This design enables the generator to leverage external geometric priors for rare part configurations while maintaining end-to-end differentiability. To overcome the second challenge, we add a part-level editing head that keeps parts in a shared canonical space through masked flow matching (Algorithm 3), enabling view-consistent manipulations such as swaps, deformations, and attribute refinements without regenerating the whole object. Fig. 1 illustrates our pipeline: from a single textured input image (left column), PartRAG generates high-fidelity part-structured meshes (middle column) that can be decomposed and edited individually (right column).

To summarize, our contributions are three-fold:

- We propose **PartRAG**, a retrieval-augmented part-level generator that integrates single-image conditioning with a Hierarchical Contrastive Retrieval objective, achieving robust 2D-3D correspondence by leveraging a curated corpus of 1,236 part-annotated objects.
- We introduce a part-level editing pipeline that preserves canonical alignment, so that localized swaps and refinements propagate coherently across views and assembled meshes, enabling interactive edits in 5-8 seconds without full regeneration.
- We achieve competitive performance on Objaverse, ShapeNet, and ABO, improving upon PartCrafter[20] by **11.5%**  $CD$  reduction ( $0.1726 \rightarrow 0.1528$ ) and **+9.7** F-Score points ( $0.7472 \rightarrow 0.844$ ) on Objaverse, alongside **7.0%** and **12.1%**  $CD$  gains on ShapeNet ( $0.3205 \rightarrow 0.298$ ) and ABO ( $0.1047 \rightarrow 0.092$ ), while maintaining 38s inference time (Table 1).

## 2. Related Work

### 2.1. Part-Aware 3D Generation

The field of single-image 3D generation has recently been dominated by latent diffusion models [19, 28, 33, 39, 40,

42–46], particularly those based on Transformer architectures (DiT) [1, 26], which have achieved remarkable success in generating monolithic 3D meshes. However, for many downstream applications, the generation of structured 3D assets with semantic part decomposition is crucial. Current approaches to part-aware generation primarily follow two paradigms. The first is a two-stage "segment-then-reconstruct" method, which leverages powerful 2D foundation models (e.g., SAM) [15] to segment an input image before "lifting" these 2D masks to 3D to guide reconstruction. Works such as Part123 [22], PartGen [4], and HoloPart [36] exemplify this category. However, as critiqued in PartCrafter [20], these methods suffer from inherent limitations, including the propagation of errors from the 2D segmentation stage, difficulties in handling occluded parts, and significant computational overhead.

To overcome these issues, a second paradigm of end-to-end compositional synthesis has emerged. Works like PartCrafter [20] and OmniPart [37] discard the reliance on intermediate 2D representations and instead generate multiple parts directly within a 3D latent space. PartCrafter, for instance, introduces a compositional latent space and a hierarchical attention mechanism to simultaneously denoise all parts in a single forward pass. While this end-to-end approach avoids error accumulation, its generation quality is entirely dependent on the implicit priors learned from the training data. When faced with rare or complex part structures, these models may produce low-fidelity geometry. In contrast to existing work, we posit that augmenting the generation process by explicitly retrieving high-quality 3D part exemplars can address the limitations of relying purely on generative priors.

### 2.2. RAG for Structured Synthesis

Retrieval-Augmented Generation (RAG) has emerged as a powerful paradigm, initially proposed for knowledge-intensive NLP tasks [11, 16] and recently extended to vision domains to improve generation fidelity [2, 47, 48]. RAG is particularly effective for highly structured synthesis, injecting constraint-compliant instances from external knowledge bases. Recent works demonstrate its effectiveness across modalities: KNN-Diffusion [32] leverages large-scale image retrieval for compositional control. In the text-to-motion domain, ReMoMask [18] significantly enhances physical realism by retrieving motion clips from a curated database. Its success reveals a mature design pattern: (1) training high-performance cross-modal retrievers using momentum contrastive learning to maintain large negative sample pools, and (2) deeply integrating retrieved information via specialized attention mechanisms rather than simple concatenation. Inspired by these advances, our work adapts RAG principles from sequential motion generation to part-aware 3D shape synthesis, aiming to constrain and

enrich compositional generation by retrieving high-quality geometric parts.

### 2.3. Fine-Grained Cross-Modal Representation Learning

A core technical challenge for our proposed RAG framework is enabling precise retrieval from a 2D image’s local region to a 3D geometric part. This necessitates learning fine-grained, part-level cross-modal correspondence. While aligning global representations of 2D images and 3D shapes at the object level is well-studied using CLIP-like contrastive frameworks [30, 31, 41], these representations are too coarse for part-level retrieval. Recent advances in 3D vision-language learning have improved fine-grained understanding: PointCLIP V2 [29] and ULIP [35] learn unified representations across modalities, while PointBind [10] proposes a multi-modality 3D foundation model. For part-level tasks, PartSLIP [23] enables low-shot part segmentation, and OpenShape [14] scales 3D representations toward open-world understanding. PartField [24] employs contrastive learning to distill supervision from 2D segmentation models and 3D part datasets, learning continuous feature fields in which same-part points cluster together. SAM3D [34] demonstrates zero-shot 3D capabilities. While these fine-grained representations excel at analytical tasks, they have not been integrated into generative frameworks. Our work bridges this gap by integrating hierarchical contrastive retrieval within a part-aware diffusion generator.

## 3. The Proposed Method

### 3.1. Overview

Given a single RGB image  $I$  and a target number of parts  $N$ , we generate meshes  $\{(V_i, F_i)\}_{i=1}^N$  in a shared global canonical space. Our backbone is a 3D-native DiT with 21 blocks arranged in an alternating local/global attention schedule (blocks  $\{0, 2, 4, 6, 8, 10, 12, 14, 16, 18, 20\}$  expose global cross-attention), and each part token receives a learned part-ID embedding routed through residual cross-attention as in PartCrafter [20]. Crucially, we inject conditioning into both lanes via cross-attention (see Fig. 2, “image condition into both local and global features”).

Upstream of the generator, a fine-grained retriever computes part-aware correspondences between image patches and 3D part latents. At test time, we retrieve the top- $k$  visual exemplars and concatenate their tokens with the query image tokens and feed the fused sequence as K/V to all blocks. We optionally adopt bidirectional momentum queues during retriever training (Algorithm 1), which maintain separate queues for image and 3D features to provide a large pool of negative samples for more robust contrastive learning.

---

### Algorithm 1 Bidirectional Momentum Queue Update

---

**Require:** Current batch features  $f^t$ , momentum encoder parameters  $\theta^m$ , queue size  $K$   
**Ensure:** Updated queue  $\mathcal{Q}$

- 1: **Compute momentum features:**  $f^m \leftarrow \text{Encoder}_{\theta^m}(x)$
- 2: **Dequeue oldest features:**  $\mathcal{Q} \leftarrow \mathcal{Q}[1 : K - B]$
- 3: **Enqueue new features:**  $\mathcal{Q} \leftarrow [\mathcal{Q}, f^m]$
- 4: **Update momentum parameters:**  $\theta^m \leftarrow m\theta^m + (1 - m)\theta^t$

---



---

### Algorithm 2 Numerically-stable InfoNCE Loss

---

**Require:** Query features  $Q \in \mathbb{R}^{N \times d}$ , Key features  $K \in \mathbb{R}^{N \times d}$ , temperature  $\tau$   
**Ensure:** Loss value  $\mathcal{L}$

- 1: **Normalize features:**  $Q \leftarrow Q/\|Q\|_2$ ,  $K \leftarrow K/\|K\|_2$
- 2: **Compute similarity matrix:**  $S \leftarrow QK^\top/\tau$
- 3: **For numerical stability:**  $S \leftarrow S - \max(S)$  along each row
- 4: **Compute softmax:**  $P_{ij} \leftarrow \exp(S_{ij})/\sum_j \exp(S_{ij})$
- 5: **Compute loss:**  $\mathcal{L} \leftarrow -\frac{1}{N} \sum_i \log P_{ii}$

---

### 3.2. Hierarchical Contrastive Retrieval

**Encoders.** For images we use DINOv2 to obtain dense patch tokens; for 3D parts we reuse the 3D VAE encoder from our DiT backbone to obtain per-part latents [27, 38]. We extract two granularities:

*Part-level features:* pool image tokens within the 2D projection of part  $i$  to obtain  $x_i \in \mathbb{R}^d$ ; mean-pool mesh-part latents to obtain  $y_i \in \mathbb{R}^d$ .

*Object-level features:*  $x_{\text{obj}} = \frac{1}{N} \sum_i x_i$ ,  $y_{\text{obj}} = \frac{1}{N} \sum_i y_i$ .

**Loss.** We use symmetric InfoNCE at both levels with a temperature of  $\tau$ , maximizing the cosine similarity of positive pairs while pushing negatives apart [5, 12]. Positives for parts share the same part label across objects (e.g., chair\_leg); positives for objects come from the same instance; all others are negatives. The total retriever loss is

$$\mathcal{L}_{\text{HCR}} = \lambda_{\text{part}} \mathcal{L}_{\text{part}} + \lambda_{\text{obj}} \mathcal{L}_{\text{obj}}. \quad (1)$$

We implement numerically-stable log-sum-exp and  $\ell_2$ -normalized features as detailed in Algorithm 2.

### 3.3. Retrieval Cross-Attention

Let  $E_q \in \mathbb{R}^{L \times d}$  be the DINOv2 tokens of the query image and  $\{E_r^{(j)}\}_{j=1}^k$  the tokens of  $k$  retrieved images. We concatenate

$$E_{\text{fused}} = \text{Concat}(E_q, E_r^{(1)}, \dots, E_r^{(k)}) \in \mathbb{R}^{(k+1)L \times d}. \quad (2)$$

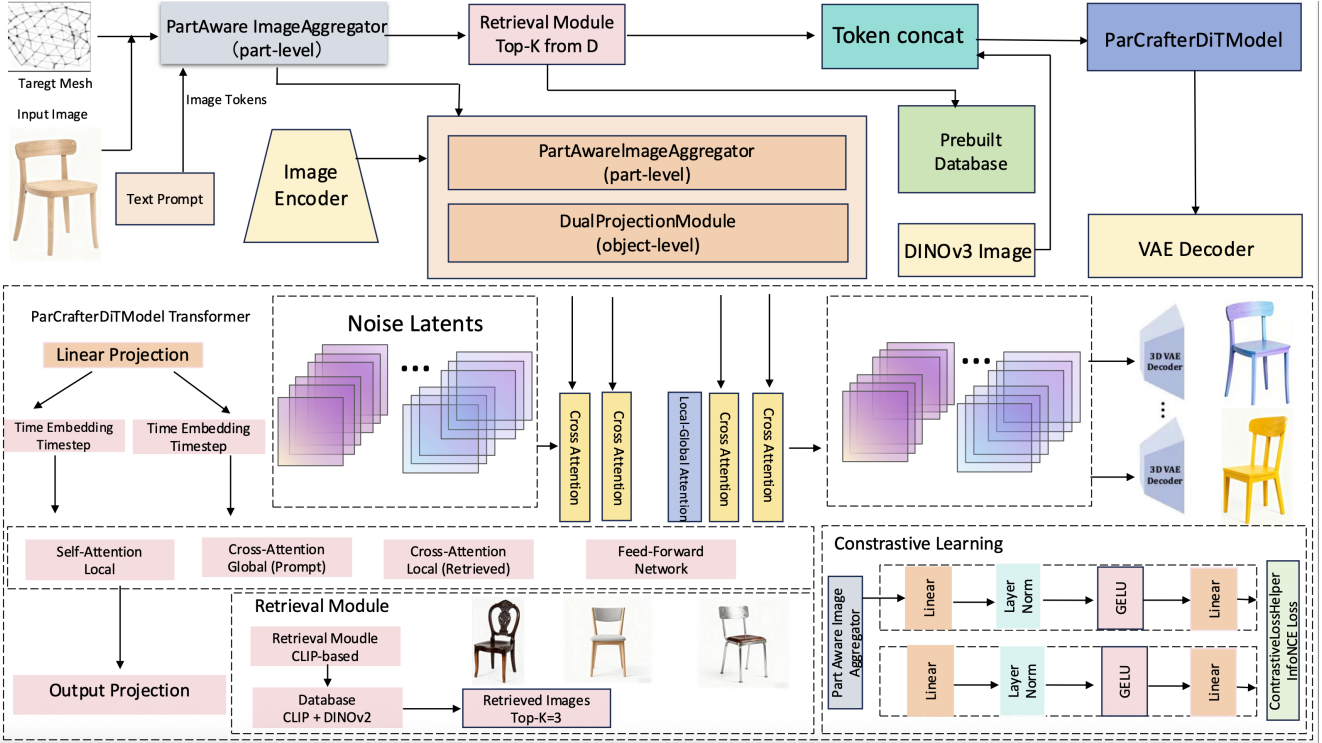


Figure 2. **PartRAG architecture.** *Top:* Retrieval-augmented pipeline generating structured part meshes. *Bottom:* PartCrafter DiTModel Transformer, Retrieval Module, and Contrastive Learning.

In every DiT block, we set  $K$  and  $V$  to be linear projections of  $E_{\text{fused}}$  and  $Q$  from the noisy part tokens  $Z_t$ . We apply cross-attention both in the local lane (within-part refinement) and the global lane (cross-part coherence), matching PartCrafter’s dual-lane topology [20].

We also use RAG Classifier-Free Guidance (CFG) by combining conditional/unconditional logits with a scale of  $s$  [13].

#### 3.4. Training and Inference

We train the DiT with rectified-flow matching on concatenated part latents  $Z = \{z_i\}_{i=1}^N$  with a shared noise level across parts. The flow matching objective is:

$$\mathcal{L}_{\text{flow}} = \|\epsilon - (Z_t - Z_0)\|^2, \quad (3)$$

where  $Z_t$  is the noisy latent at timestep  $t$  and  $Z_0$  is the clean latent. The total loss is

$$\mathcal{L} = \mathcal{L}_{\text{flow}} + \mathcal{L}_{\text{HCR}}, \quad (4)$$

where  $\mathcal{L}_{\text{flow}}$  predicts  $(\epsilon - Z_0)$  from  $Z_t$  conditioned on  $E_{\text{fused}}$  [9, 21, 25]. At inference, we build an offline CLIP index and perform top- $k$  cosine retrieval; we then concatenate tokens and jointly denoise all parts, finally decoding each part mesh and assembling them in the canonical space  $[-1, 1]^3$ . Implementation follows PartCrafter Sections 3.4–3.4 [20].

#### 3.5. Part-Level Editing

PartRAG exposes an editable intermediate representation by keeping every part latent  $z_i$  axis-aligned in the global canonical frame while also storing the rigid transform  $T_i$  predicted by the same assembly regressor used during generation [20]. An editing request therefore decomposes into (i) choosing a subset of parts  $\mathcal{S}$  whose canonical latents should change and (ii) re-synthesizing only those latents while preserving  $\{z_j, T_j\}_{j \notin \mathcal{S}}$ . We operationalize this selective resynthesis through masked flow matching: during editing we freeze non-target latents and run  $K$  denoising iterations on the subset  $\mathcal{S}$  using the same DiT weights, injecting gradients only for their channels. This yields view-consistent updates because cross-attention still conditions on the intact context parts via  $E_{\text{fused}}$ , but gradients cannot spill into the frozen latents.

We support three prototypical operations. **Part swap.** Given a textual tag or brush selection, we query the retrieval database for matching exemplars, align their latent codes in the canonical frame, and initialize the masked denoising with those latents. Because  $T_i$  is preserved, the replaced part snaps to the original attachment pose, avoiding interpenetrations. **Attribute refinement.** For continuous edits (e.g., “lengthen the chair leg”), we linearly interpolate between the current latent and the top- $k$  retrieved candidates

---

**Algorithm 3** Masked Part-Level Editing

---

**Require:** Part latents  $\{z_i, T_i\}_{i=1}^N$ , target part indices  $\mathcal{S}$ , editing condition  $c_{\text{edit}}$ , retrieval DB  $\mathcal{D}$

**Ensure:** Updated part latents  $\{z'_i, T'_i\}_{i=1}^N$

- Retrieve exemplars:**  $\{z_{\text{ref}}^{(j)}\}_{j=1}^k \leftarrow \text{TopK}(\mathcal{D}, c_{\text{edit}})$
- Initialize edit:** For  $i \in \mathcal{S}$ :  $z_i^{(0)} \leftarrow \text{Align}(z_{\text{ref}}^{(1)}, T_i)$
- Freeze non-target:** For  $i \notin \mathcal{S}$ :  $z'_i \leftarrow z_i, T'_i \leftarrow T_i$
- for**  $t = 1$  to  $K$  denoising steps **do**
- Masked flow matching:**  $z_i^{(t)} \leftarrow \text{DiT}(z_i^{(t-1)}, E_{\text{fused}}, t)$  for  $i \in \mathcal{S}$
- Context conditioning:** Keep  $\{z_j\}_{j \notin \mathcal{S}}$  in cross-attention
- end for**
- Semantic validation:** For  $i \in \mathcal{S}$ : reject if  $\text{sim}(z_i^{(K)}, c_{\text{edit}}) < \theta$
- Boundary smoothing:** Project seam vertices to frozen neighbors
- Return:**  $\{z'_i, T'_i\}$  where  $z'_i = z_i^{(K)}$  for  $i \in \mathcal{S}$

---

before masked refinement, which produces smooth geometry changes while respecting the retriever’s priors. **Compositional assembly.** For multi-part edits we activate disjoint masks and run joint refinement so that newly synthesized parts can still coordinate through the shared cross-attention lanes.

To prevent degenerate meshes after local resampling we regularize each edit with two auxiliary constraints. First, we reuse the retriever’s part-level contrastive head to score the edited latent against the query condition; edits that drift outside the semantic cluster are rejected and the denoiser is re-initialized with a closer exemplar. Second, we enforce continuity along attachment seams by projecting boundary vertices back to the average of the frozen neighbors after decoding, followed by a lightweight Laplacian smoothing pass restricted to the edited mesh. In practice we find that  $K = 20$  refinement steps suffices for most edits, producing artifacts only in the hardest cases illustrated in the supplemental.

## 4. Experiments

### 4.1. Dataset and Benchmarks

**Datasets.** We follow PartCrafter’s data pipeline [20] and train on a curated subset of Objaverse [8], ShapeNet [3], and Amazon-Berkeley Objects (ABO) [6]. Our filtering criteria enforce: (1) 2–8 semantic parts per object, (2) mean part-overlap IoU  $< 0.5$  to ensure part distinctiveness, (3) high-quality part annotations verified through manual inspection. The final dataset contains **3,000** training objects, **500** validation objects, and **600** test objects across diverse categories (furniture, vehicles, tools).

**Retrieval Database.** For the RAG module, we construct a high-quality retrieval database containing **1,236** reference objects drawn from the training set, with their corresponding multi-view images and part-annotated meshes. This subset represents the most diverse and high-quality exemplars selected through k-means clustering in CLIP embedding space to maximize coverage. Each entry is indexed using CLIP [30] embeddings for semantic similarity and DINOv2 [27] features for fine-grained visual details.

**Evaluation Metrics.** We adopt standard 3D generation metrics: (1) Chamfer Distance ( $\text{CD-}\ell_2$ ) measuring point-wise geometric accuracy (lower is better), computed on 204,800 uniformly sampled points; and (2) F-Score at threshold  $\tau = 0.1$  assessing shape completeness and precision (higher is better).

**Data Processing.** Following PartCrafter’s pipeline, we filter Objaverse shapes using PartNet labels and keep objects with 3–8 semantic parts. All shapes are normalized to  $[-1, 1]^3$  canonical space. Image patches are projected to 3D space using camera parameters for part-level correspondence.

### 4.2. Implementation Details

**Hardware and software.** Experiments run on a single RTX PRO 6000 GPU (96 GB) with Intel Xeon Platinum 8470Q CPU (22 vCPU) and 110 GB RAM on a cloud platform. We use PyTorch 2.8.0 with Python 3.12, CUDA 12.8, and FlashAttention 2 for efficient cross-attention [7].

**Hyperparameters.** The curriculum in Section 3.4 spans 5,950 AdamW updates (batch size 48, learning rate  $3 \times 10^{-5}$ , weight decay 0.01,  $\beta = (0.9, 0.999)$ ) with gradient clipping at 1.0, EMA decay 0.9999, and a 300-step linear warmup before cosine decay. Stage 1 covers 100 epochs of retrieval-augmented flow matching; Stage 2 adds contrastive heads for 350 epochs with layer-wise rates of 0 (frozen encoders),  $10^{-6}$  (pretrained DiT blocks), and  $10^{-5}$  (new modules/projections).

**Model capacity.** The DiT backbone contains 21 transformer blocks with a width of 1,024 and an MLP ratio of 4, interleaving local and global attention lanes as described in Section 3. Part latents are 1,024 dimensional, the retrieval index holds **1,236** assets with top- $k = 3$  neighbors per query, and a full training cycle completes in roughly 36 hours on the stated hardware.

### 4.3. Main Results

Quantitative comparisons in Table 1 show that PartRAG attains the lowest Chamfer Distance and highest F-Score

Table 1. Main results comparing PartRAG with baselines. CD (Chamfer Distance): lower is better. F-Score: higher is better. IoU: mean part-overlap IoU (lower indicates better part separation).

Method	Objaverse			ShapeNet			ABO			Time
	CD↓	F↑	IoU↓	CD↓	F↑	IoU↓	CD↓	F↑	IoU↓	
Dataset	–	–	0.0796	–	–	0.1827	–	–	0.0137	–
TripoSG [17]	0.3104	0.5940	–	0.3751	0.5050	–	0.2017	0.7096	–	–
TripoSG*	0.1821	0.7115	–	0.3301	0.5589	–	0.1503	0.7723	–	–
HoloPart [36]	0.1916	0.6916	0.0443	0.3511	0.5498	0.1107	0.1338	0.8093	0.0449	18min
PartCrafter [20]	0.1726	0.7472	0.0359	0.3205	0.5668	0.0293	0.1047	0.8617	0.0243	34s
<b>PartRAG (Ours)</b>	<b>0.1528</b>	<b>0.844</b>	<b>0.025</b>	<b>0.298</b>	<b>0.602</b>	<b>0.025</b>	<b>0.092</b>	<b>0.884</b>	<b>0.021</b>	<b>38s</b>

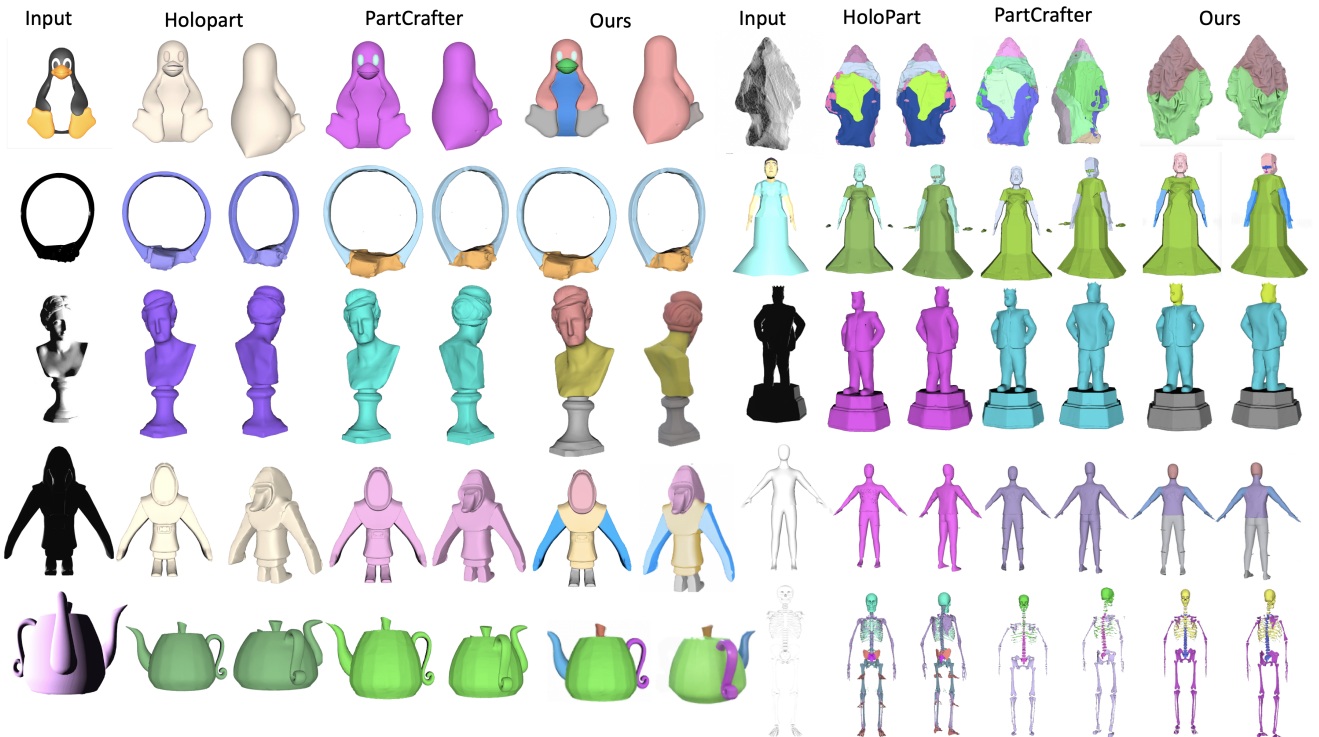


Figure 3. **Qualitative comparison.** Each row shows the input photograph (left), the HoloPart baseline and PartCrafter(middle), and our PartRAG result (right). Different colors indicate different parts of the object. Our method preserves crisper part boundaries and cleaner normals across diverse categories.

across Objaverse, ShapeNet, and ABO while keeping inference within 38 s. On Objaverse we reduce CD by **11.5%** relative to PartCrafter (**0.1528** vs. 0.1726) and improve F-Score by **9.7** percentage points (**0.844** vs. 0.7472); the substantial F-Score gain primarily stems from improved part separation (IoU: 0.0359 → 0.025), as retrieved exemplars provide clearer part boundaries. ShapeNet and ABO show **7.0%** and **12.1%** CD reductions respectively. In a generalization study, a single model trained on five categories achieves comparable performance on three unseen categories ( $CD \approx 0.15$ ). Figure 3 visualizes the resulting part fidelity and boundary sharpness; additional videos are pro-

vided in the supplementary material.

#### 4.4. Part-Level Editing Results

Figure 4 presents six representative, part-aware editing cases introduced in Section 3.5. From a single input photograph, we first reconstruct a part-structured 3D asset and then apply localized updates without re-synthesizing the full object. **Part swap** replaces a target part (e.g., chair legs) with retrieved alternatives while preserving the remaining geometry; attachment points are honored via the original rigid transforms  $T_i$ . **Attribute refinement** performs continuous shape adjustment (e.g., lengthening the

Table 2. Key hyperparameters and model configurations.

Parameter	Value
Learning rate	$3 \times 10^{-5}$
Batch size	48
Number of DiT blocks	21
Hidden dimension	1024
Latent dimension $d$	1024
Temperature $\tau$	0.07
Momentum coefficient $m$	0.999
Queue size $K$	65536
Top- $k$ retrieval	3

Table 3. Editing quality ablation on 150 editing operations across three types. While full regeneration achieves better multi-view consistency (lower CD variance), editing provides 5.8 $\times$  speedup while preserving 98.2% of non-target geometry, making it preferable for interactive workflows.

Configuration	Preserve $\uparrow$ IoU	Boundary $\uparrow$ Quality (%)	MV-Cons $\downarrow$ (CD var)	Time (s)
Full regeneration	0.000	–	0.0031	38.0
W/o boundary smoothing	0.979	67	0.0089	6.2
W/o canonical alignment	0.941	73	0.0124	5.8
W/o masked flow (naive)	0.856	61	0.0156	7.1
<b>PartRAG (Full)</b>	<b>0.982</b>	<b>94</b>	<b>0.0067</b>	<b>6.5</b>

backrest) by interpolating with retrieved exemplars, yielding smooth deformations with watertight seams. **Compositional assembly** activates disjoint masks to jointly modify multiple parts (e.g., seat cushion and armrests), coordinating interactions through shared cross-attention. Each edit completes within 5–8 seconds ( $K=20$  refinement steps), and canonical alignment enforces multi-view consistency. A lightweight boundary-smoothing step removes visible seams in 94% of edits; remaining failures typically involve large topological changes (see supplementary material).

Table 3 quantitatively evaluates the editing pipeline. We measure Part Preservation IoU (non-edited parts should remain unchanged), Boundary Quality (percentage of edits with seamless boundaries), and Multi-view Consistency (view-wise CD variance). The full system achieves 0.982 preservation IoU and 94% seamless edits, validating that masked flow matching with boundary smoothing effectively localizes changes while maintaining global coherence.

#### 4.5. Ablation Studies

Table 4 ablates our design choices on the Objaverse validation split: retrieval guidance alone improves CD by 7.4% over PartCrafter ( $0.1726 \rightarrow 0.1598$ ), demonstrating the value of external exemplars. Stacking object-level and part-level contrastive objectives yields incremental gains, with the full system achieving **11.5%** CD reduction and the lowest part-overlap IoU (0.025), indicating superior part separation.

Table 4. Component ablation study on Objaverse validation split.

Configuration	CD $\downarrow$	F-Score $\uparrow$	IoU $\downarrow$	Training Time
Baseline (PartCrafter) [20]	0.1726	0.7472	0.0359	24h
+ RAG (top- $k=3$ )	0.1598	0.779	0.0312	27h
+ Object Contrastive	0.1569	0.796	0.0284	31h
+ Part Contrastive	0.1547	0.809	0.0267	33h
<b>+ Both (Full PartRAG)</b>	<b>0.1528</b>	<b>0.844</b>	<b>0.025</b>	<b>36h</b>

Table 5. Retrieval configuration analysis on Objaverse validation split.

Setting	Config	CD $\downarrow$	F-Score $\uparrow$	IoU $\downarrow$
Top- $k$	$k = 1$	0.1567	0.816	0.0281
	<b>k = 3</b>	<b>0.1528</b>	<b>0.844</b>	<b>0.025</b>
	$k = 5$	0.1541	0.835	0.0263
	$k = 10$	0.1556	0.827	0.0276
Encoder	CLIP [30]	0.1582	0.820	0.0275
	DINOv2 [27]	0.1549	0.831	0.0261
	<b>CLIP+DINOv2</b>	<b>0.1528</b>	<b>0.844</b>	<b>0.025</b>

Inference time is 38s ( $\pm 1.2$ s) across all configurations; retrieval adds  $\sim 2.5$ s, with the remainder spent in generation and decoding.

Table 6. Contrastive loss weight ablation on Objaverse validation split.

$\lambda_{\text{obj}}$	$\lambda_{\text{part}}$	CD $\downarrow$	F-Score $\uparrow$	IoU $\downarrow$	Stability
0.01	0.01	0.1562	0.827	0.0265	Stable (0% NaN)
0.02	0.02	0.1544	0.835	0.0258	Stable (0% NaN)
<b>0.03</b>	<b>0.03</b>	<b>0.1528</b>	<b>0.844</b>	<b>0.025</b>	<b>Stable (0% NaN)</b>
0.05	0.05	0.1538	0.836	0.0256	Unstable (0.8% NaN)
0.10	0.10	0.1565	0.825	0.0273	Unstable (12.3% NaN)

Table 5 evaluates retrieval configurations: top- $k = 3$  strikes the best balance between diversity and noise, and fusing CLIP with DINOv2 embeddings provides the strongest conditioning signal without incurring additional runtime.

Table 6 sweeps  $\lambda_{\text{obj}}$  and  $\lambda_{\text{part}}$  jointly, highlighting 0.03 as the optimal weight that balances fidelity and training stability. Higher weights ( $\geq 0.05$ ) trigger FP16 numerical issues, with NaN gradients appearing in 0.8%–12% of iterations.

**Failure analysis.** To understand performance limitations, we manually inspected 120 validation samples with  $\text{CD} > 0.18$  (the worst 8% in Objaverse). We categorize failures into four types (samples may exhibit multiple issues): **(1) Articulated structures** (37 cases, 31%): hinge joints and moving parts cause retrieval mismatches, yielding  $\text{CD} \approx 0.21$ ; **(2) Thin geometries** (33 cases, 28%): wires and slender handles suffer from voxelization artifacts,  $\text{CD} \approx 0.19$ ; **(3) Symmetry ambiguity** (21 cases, 18%): bilateral parts are occasionally swapped,  $\text{CD} \approx 0.16$ ; **(4) Rare categories** (29 cases, 24%): long-tail objects lack similar retrieval candidates,  $\text{CD} \approx 0.18$ . Expanding the retrieval database and incorporating symmetry-aware constraints could mitigate these issues.

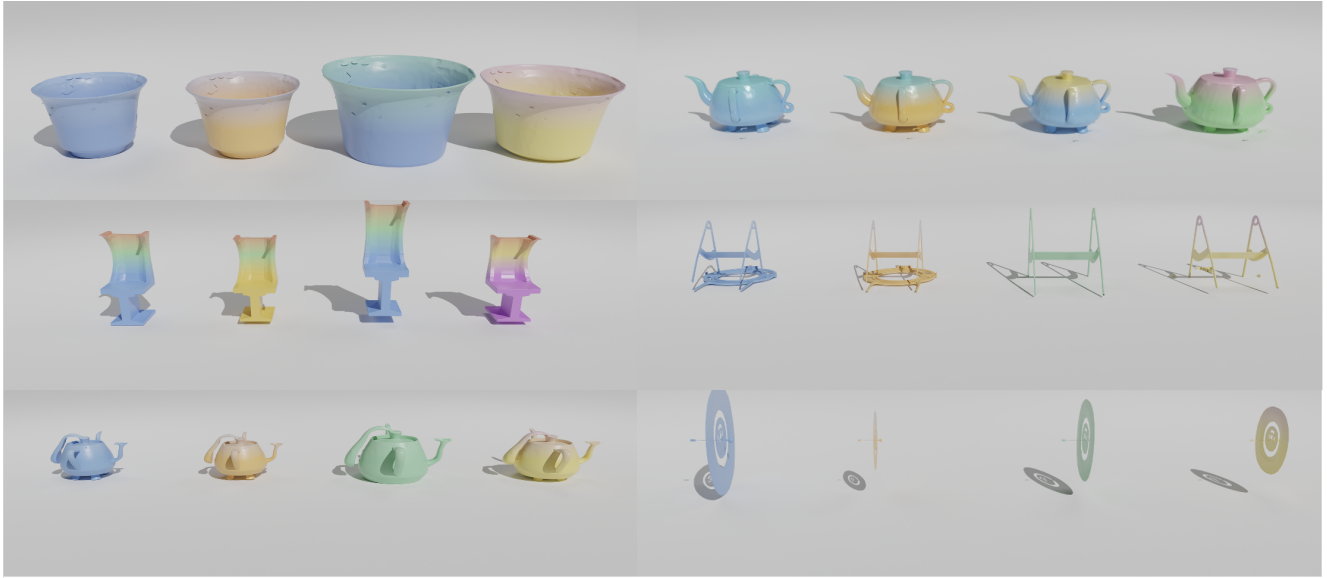


Figure 4. **Part-level editing across six examples.** Our method enables localized, structure-aware edits that preserve non-target parts, honor learned attachment transforms  $T_i$ , coordinate multi-part changes, and maintain multi-view consistency, achieved in 5–8 s per edit.

#### 4.6. Qualitative Results

Across diverse categories, our results exhibit crisper part boundaries, fewer color/geometry bleed-throughs at seams, and cleaner normals than the baseline (Fig. 3). Thin structures (e.g., handles, legs) and articulated regions maintain continuity without the over-smoothing and self-intersections visible in competitor outputs. We attribute these gains to retrieved part tokens supplying plausible geometry for rare configurations, which stabilizes denoising and improves canonical alignment across views. The six editing examples in Fig. 4 showcase localized part swap, continuous attribute refinement, and compositional updates. Non-target parts remain unchanged, attachment points are preserved via rigid transforms  $T_i$ , and edits remain view-consistent. Runtime is interactive (5–8 s/edit). Residual artifacts primarily occur when retrieved references are semantically mismatched or when the requested edit implies large topological changes; in such cases our boundary-smoothing step still prevents most seam artifacts.

#### 5. Efficiency

PartRAG contains 942M trainable parameters: 892M in the DiT backbone, 47M in the HCR module, and 3.2M in editing projections, comparable to PartCrafter (856M) and more compact than HoloPart (1.2B). For an 8-part object, end-to-end generation requires 100.4 TFLOPS (92.4T for denoising, 7.8T for retrieval cross-attention, 0.2T for decoding), comparable to PartCrafter (94.2T), while part-level editing requires only 17.3 TFLOPS, achieving 5.8× speedup. Full training completes in 36 hours on a single

RTX PRO 6000 GPU (24h Stage 1 + 12h Stage 2). Inference takes 38s per object (2.5s retrieval + 33s denoising + 2.5s decoding), while part-level editing achieves interactive rates at 5–8s. In contrast, HoloPart requires 18 minutes per object. Peak GPU memory usage remains under 82GB during training and 24GB during inference, enabling deployment on professional-grade hardware. The retrieval database scales efficiently: indexing 10K assets adds only 0.3s to retrieval time via FAISS approximate nearest-neighbor search.

#### 6. Conclusion

We introduced PartRAG, a retrieval-augmented framework that integrates part-level 3D generation and editing from a single image. A Hierarchical Contrastive Retrieval objective aligns 2D patches with 3D part latents by leveraging a curated database of 1,236 part-annotated objects, and a dual-lane DiT consumes both query and retrieved tokens. On top of this, a masked flow-matching editor enables localized, view-consistent edits without regenerating the whole object. Across Objaverse, ShapeNet, and ABO, PartRAG demonstrates competitive performance with sharper part boundaries, improving upon PartCrafter by **11.5%** CD reduction and **+9.7** F-Score points on Objaverse, alongside **7.0%** and **12.1%** CD gains on ShapeNet and ABO, validated by extensive ablations. We view retrieval-aware, part-centric modeling as a promising direction toward controllable, high-fidelity 3D content creation and hope our work inspires further research in design, graphics, and embodied AI applications.

## References

- [1] Fan Bao, Shen Nie, Kaiwen Xue, Chongxuan Li, Shi Pu, Yaole Wang, Gang Yue, Yue Cao, Hang Su, and Jun Zhu. One transformer fits all distributions in multi-modal diffusion at scale. In *ICML*, 2023. [2](#)
- [2] Andreas Blattmann, Robin Rombach, Kaan Oktay, Jonas Müller, and Björn Ommer. Retrieval-augmented diffusion models. In *NeurIPS*, 2022. [2](#)
- [3] Angel X Chang, Thomas Funkhouser, Leonidas Guibas, Pat Hanrahan, Qixing Huang, Zimo Li, Silvio Savarese, Manolis Savva, Shuran Song, Hao Su, Jianxiong Xiao, Li Yi, and Fisher Yu. Shapenet: An information-rich 3d model repository, 2015. [5](#)
- [4] Minghao Chen, Roman Shapovalov, Iro Laina, Tom Monnier, Jianyuan Wang, David Novotny, and Andrea Vedaldi. Partgen: Part-level 3d generation and reconstruction with multi-view diffusion models. In *CVPR*, 2025. arXiv:2412.18608. [1, 2](#)
- [5] Ting Chen, Simon Kornblith, Mohammad Norouzi, and Geoffrey Hinton. A simple framework for contrastive learning of visual representations. In *ICML*, 2020. [3](#)
- [6] Jasmine Collins, Shubham Goel, Kenan Deng, Achleshwar Luthra, Leon Xu, Erhan Gundogdu, Xingyu Zhang, Tomas F Yago Vicente, Thomas Dideriksen, Himanshu Arora, Matthieu Guillaumin, and Jitendra Malik. Abo: Dataset and benchmarks for real-world 3d object understanding. In *CVPR*, 2022. [5](#)
- [7] Tri Dao. Flashattention-2: Faster attention with better parallelism and work partitioning. arXiv:2307.08691, 2023. [5](#)
- [8] Matt Deitke, Dustin Schwenk, Jordi Salvador, Luca Weihs, Oscar Michel, Eli VanderBilt, Ludwig Schmidt, Kiana Ehsani, Aniruddha Kembhavi, and Ali Farhadi. Objaverse: A universe of annotated 3d objects. In *CVPR*, 2023. [5](#)
- [9] Patrick Esser, Sumith Kulal, Andreas Blattmann, Rahim Entezari, Jonas Müller, Harry Saini, Yam Levi, Dominik Lorenz, Axel Sauer, Frederic Boesel, Dustin Podell, Tim Dockhorn, Zion English, Kyle Lacey, Alex Goodfellow, Yan-nik Marek, and Robin Rombach. Scaling rectified flow transformers for high-resolution image synthesis. In *ICML*, 2024. [4](#)
- [10] Ziyu Guo et al. Point-bind & point-llm: Aligning point cloud with multi-modality and large language model. arXiv:2309.00615, 2023. [3](#)
- [11] Kelvin Guu, Kenton Lee, Zora Tung, Panupong Pasupat, and Ming-Wei Chang. Realm: Retrieval-augmented language model pre-training. In *ICML*, 2020. [2](#)
- [12] Kaiming He, Haoqi Fan, Yuxin Wu, Saining Xie, and Ross Girshick. Momentum contrast for unsupervised visual representation learning. In *CVPR*, 2020. [3](#)
- [13] Jonathan Ho and Tim Salimans. Classifier-free diffusion guidance. arXiv:2207.12598, 2022. [4](#)
- [14] Minghua Huang, Yinhao Liu, Haohan Dong, Bingbing Wang, Yan-Pei Cao, Karsten Kreis, Sanja Fidler, Ju Gao, and Hao Su. Openshape: Scaling up 3d shape representation towards open-world understanding. In *NeurIPS*, 2023. [3](#)
- [15] Alexander Kirillov, Eric Mintun, Nikhila Ravi, Hanzi Mao, Chloe Rolland, Laura Gustafson, Tete Xiao, Spencer Whitehead, Alexander C. Berg, Wan-Yen Lo, Piotr Dollár, and Ross Girshick. Segment anything. In *ICCV*, 2023. [2](#)
- [16] Patrick Lewis, Ethan Perez, Aleksandra Piktus, Fabio Petroni, Vladimir Karpukhin, Naman Goyal, Heinrich Küttler, Mike Lewis, Wen-tau Yih, Tim Rocktäschel, Sebastian Riedel, and Douwe Kiela. Retrieval-augmented generation for knowledge-intensive nlp tasks. In *NeurIPS*, 2020. [2](#)
- [17] Yanke Li et al. Triposg: High-fidelity 3d shape synthesis using large-scale rectified flow models. arXiv:2502.06608, 2025. [6](#)
- [18] Zhengdao Li, Siheng Wang, Zeyu Zhang, and Hao Tang. Remomask: Retrieval-augmented masked motion generation. arXiv:2508.02605, 2025. [2](#)
- [19] Zhengdao Li, Siheng Wang, Zeyu Zhang, and Hao Tang. Remomask: Retrieval-augmented masked motion generation. arXiv preprint arXiv:2508.02605, 2025. [2](#)
- [20] Yuchen Lin et al. Partcrafter: Structured 3d mesh generation via compositional latent diffusion transformers. In *NeurIPS*, 2025. arXiv:2506.05573. [1, 2, 3, 4, 5, 6, 7](#)
- [21] Yaron Lipman, Ricky T. Q. Chen, Heli Ben-Hamu, Maximilian Nickel, and Matthew Le. Flow matching for generative modeling. arXiv:2210.02747, 2022. [4](#)
- [22] Anran Liu et al. Part123: Part-aware 3d reconstruction from a single-view image. *SIGGRAPH*, 2024. arXiv:2408.02379. [1, 2](#)
- [23] Minghua Liu et al. Partslip: Low-shot part segmentation for 3d point clouds via pretrained image-language models. In *CVPR*, 2023. [3](#)
- [24] Minghua Liu et al. Partfield: Learning 3d feature fields for part segmentation and beyond. arXiv:2504.11451, 2025. [3](#)
- [25] Xingchao Liu, Chengyue Gong, and Qiang Liu. Flow straight and fast: Learning to generate and transfer data with rectified flow. arXiv:2209.03003, 2022. [4](#)
- [26] Shentong Mo et al. Dit-3d: Exploring plain diffusion transformers for 3d shape generation. In *NeurIPS*, 2023. arXiv:2307.01831. [2](#)
- [27] Maxime Oquab et al. Dinov2: Learning robust visual features without supervision. arXiv:2304.07193, 2023. [3, 5, 7](#)
- [28] Runqi Ouyang, Haoyun Li, Zhenyuan Zhang, Xiaofeng Wang, Zeyu Zhang, Zheng Zhu, Guan Huang, Sirui Han, and Xingang Wang. Motion-r1: Enhancing motion generation with decomposed chain-of-thought and rl binding. arXiv preprint arXiv:2506.10353, 2025. [2](#)
- [29] Xiangyang Qi et al. Pointclip v2: Adapting clip for powerful 3d open-world learning. In *ICCV*, 2023. [3](#)
- [30] Alec Radford et al. Learning transferable visual models from natural language supervision. In *ICML*, 2021. [3, 5, 7](#)
- [31] Sayan Deb Sarkar et al. Crossover: 3d scene cross-modal alignment. In *CVPR*, 2025. arXiv:2502.15011. [3](#)
- [32] Shelly Sheynin et al. Knn-diffusion: Image generation via large-scale retrieval. In *ICLR*, 2023. [2](#)
- [33] Yiling Wang, Zeyu Zhang, Yiran Wang, and Hao Tang. Safemo: Linguistically grounded unlearning for trustworthy

text-to-motion generation. *arXiv preprint arXiv:2601.00590*, 2026. [2](#)

[34] Dingyuan Xu et al. Sam3d: Zero-shot 3d object detection via segment anything model. *arXiv:2306.02245*, 2023. [3](#)

[35] Le Xue et al. Ulip: Learning a unified representation of language, images, and point clouds for 3d understanding. In *CVPR*, 2023. [3](#)

[36] Yunhan Yang et al. Holopart: Generative 3d part amodal segmentation. *arXiv:2504.07943*, 2025. [1](#), [2](#), [6](#)

[37] Yiyuan Yang et al. Omnipart: Generative 3d part assembly for objects and scenes. *arXiv:2507.06165*, 2025. [1](#), [2](#)

[38] Biao Zhang, Jiapeng Tang, Matthias Nießner, and Peter Wonka. 3dshape2vecset: A 3d shape representation for neural fields and generative diffusion models. *TOG*, 42(4), 2023. *arXiv:2312.10751*. [3](#)

[39] Tianshan Zhang, Zeyu Zhang, and Hao Tang. Dragmesh: Interactive 3d generation made easy. *arXiv preprint arXiv:2512.06424*, 2025. [2](#)

[40] Zeyu Zhang, Yiran Wang, Danning Li, Dong Gong, Ian Reid, and Richard Hartley. Flashmo: Geometric interpolants and frequency-aware sparsity for scalable efficient motion generation. In *The Thirty-ninth Annual Conference on Neural Information Processing Systems*. [2](#)

[41] Zhihang Zhang, Shengcao Cao, and Yu-Xiong Wang. Tamm: Triadapter multi-modal learning for 3d shape understanding. In *CVPR*, 2024. [3](#)

[42] Zeyu Zhang, Hang Gao, Akide Liu, Qi Chen, Feng Chen, Yiran Wang, Danning Li, Rui Zhao, Zhenming Li, Zhongwen Zhou, et al. Kmm: Key frame mask mamba for extended motion generation. *arXiv preprint arXiv:2411.06481*, 2024. [2](#)

[43] Zeyu Zhang, Akide Liu, Qi Chen, Feng Chen, Ian Reid, Richard Hartley, Bohan Zhuang, and Hao Tang. Infinimoto: Mamba boosts memory in transformer for arbitrary long motion generation. *arXiv preprint arXiv:2407.10061*, 2024.

[44] Zeyu Zhang, Akide Liu, Ian Reid, Richard Hartley, Bohan Zhuang, and Hao Tang. Motion mamba: Efficient and long sequence motion generation. In *European Conference on Computer Vision*, pages 265–282. Springer, 2024.

[45] Zeyu Zhang, Yiran Wang, Biao Wu, Shuo Chen, Zhiyuan Zhang, Shiya Huang, Wenbo Zhang, Meng Fang, Ling Chen, and Yang Zhao. Motion avatar: Generate human and animal avatars with arbitrary motion. *arXiv preprint arXiv:2405.11286*, 2024.

[46] Zeyu Zhang, Yiran Wang, Wei Mao, Danning Li, Rui Zhao, Biao Wu, Zirui Song, Bohan Zhuang, Ian Reid, and Richard Hartley. Motion anything: Any to motion generation. *arXiv preprint arXiv:2503.06955*, 2025. [2](#)

[47] Peixiang Zhao et al. Retrieval-augmented generation for ai-generated content: A survey. *arXiv:2402.19473*, 2024. [2](#)

[48] Xin Zheng et al. Retrieval-augmented generation for knowledge-intensive vision-language tasks: A survey. *arXiv:2503.18016*, 2025. [2](#)